Author Manuscript

Author Manuscript

Author Manuscript

Author Manuscript

HHS Public Access

Author manuscript

Matrix Biol. Author manuscript; available in PMC 2023 September 27.

Published in final edited form as:

Matrix Biol. 2023 August ; 121: 41–55. doi:10.1016/j.matbio.2023.05.004.

TGFβ−2 haploinsufficiency causes early death in mice with Marfan syndrome

Nalani Sachan[a], **Colin K.L. Phoon**[b], **Lior Zilberberg**[a,1], **Matthias C. Kugler**[c], **Taylor Ene**[a], **Shana B. Mintz**[c], **Sae-Il Murtada**[d], **Dar Weiss**[d], **Glenn I. Fishman**[c], **Jay D. Humphrey**[d], **Daniel B. Rifkin**[a,c]

[a]Department of Cell Biology, NYU Grossman School of Medicine, New York, NY 10016, USA

[b]Department of Pediatrics, NYU Grossman School of Medicine, New York, NY 10016, USA

[c]Department of Medicine, NYU Grossman School of Medicine, New York, NY 10016, USA

[d]Department of Biomedical Engineering, Yale University, New Haven, CT 06520, USA

Abstract

To assess the contribution of individual TGF-β isoforms to aortopathy in Marfan syndrome (MFS), we quantified the survival and phenotypes of mice with a combined fibrillin1 (the gene defective in MFS) hypomorphic mutation and a TGF-β1, 2, or 3 heterozygous null mutation. The loss of TGF-β2, and only TGF-β2, resulted in 80% of the double mutant animals dying earlier, by postnatal day 20, than MFS only mice. Death was not from thoracic aortic rupture, as observed in MFS mice, but was associated with hyperplastic aortic valve leaflets, aortic regurgitation, enlarged aortic root, increased heart weight, and impaired lung alveolar septation. Thus, there appears to be a relationship between loss of fibrillin1 and TGF-β2 in the postnatal development of the heart, aorta and lungs.

Keywords

TGF-β2; Marfan syndrome; Thoracic aortic aneurysms; Aortic valves; Biomechanical evaluation; Aortic regurgitation

Introduction

The transforming growth factor b (TGF-β) cytokine family members, TGF-β1, b2 and b3, have critical roles during development and homeostasis and their mis-regulation associates

This is an open access article under the CC BY-NC-ND license (http://creativecommons.org/licenses/by-nc-nd/4.0/)

Corresponding author. nalani.sachan@nyumc.org, bhunalini@gmail.com.

[1]Current address: Smidt Heart Institute, Cedars-Sinai Medical Center, Los Angeles, CA, 90,048, USA.

Author contributions

NS, LZ, CKLP, MCK, SM, GIF, JH, and DBR collected and analyzed the data. NS, JH, and DBR wrote the manuscript. JH and DBR acquired funding. All authors read and revised the paper.

Declaration of Competing Interest

All of the authors declare no conflict of interest.

Supplementary materials

Supplementary material associated with this article can be found in the online version at doi:10.1016/j.matbio.2023.05.004.

Author Manuscript Author Manuscript Author Manuscript Author Manuscript

with cancer, skeletal abnormalities, inflammatory diseases, fibrosis, and vascular conditions [1–4]. In 2003, Neptune and colleagues reported the unexpected result that blockade of TGF-β signaling in mice with MFS, an autosomal dominant condition caused by mutations in the gene *Fbn1* that codes for the extracellular matrix glycoprotein fibrilin1, ameliorated the lung pathology [5]. MFS predisposes carriers to the cardinal manifestations of thoracic aortic aneurysms (TAA), dissection, and rupture, as well as long bone overgrowth, ectopia lentis, and lung pathology [6]. The authors reasoned that because the latent TGF-β binding proteins (LTBPs) that carry latent TGF-β associate with fibrillin1, mutations that decrease matrix fibrillin1 might perturb the extracellular regulation of TGF-β, yielding enhanced growth factor signaling [5]. In support of this hypothesis, the administration of TGF-β neutralizing antibodies or the antihypertensive drug losartan, known to lower TGF-β levels, diminished aortic dilation and prolonged survival in MFS mice [7] and patients treated with losartan or related molecules [8]. Since these original publications, loss of function mutations in the genes encoding multiple components of the TGF-β signaling pathway have been found to be responsible for conditions associated with TAA. These include Loeys-Dietz syndrome (LDS) type 1 (TGF-β receptor I mutations), LDS type 2 (TGF-β receptor II mutations), LDS type 3 (SMAD2 or 3 mutations), LDS type 4 (TGF-β2 mutations), LDS type 5 (TGF-β3 mutations), and Shprintzen-Goldberg syndrome (SKI mutations) [9]. Together, these results provide evidence that perturbations in the TGF-β signaling pathway can yield abnormal thoracic aortic development and maintenance.

Further experiments have illustrated a more nuanced and complicated biology, however, as blockade of TGF-β signaling by genetic approaches in MFS mice, such as conditional deletion of *Tgfbr2,* or early treatment with TGF-β neutralizing antibodies, yielded animals with decreased, rather than increased, survival, larger aneurysms, and, in some cases, wild type (WT) mice with aneurysms [10–13]. Cook and colleagues demonstrated that the time of initiation of TGF-β blockade is crucial [14]; in a murine model with severe MFS, inhibition of TGF-β with neutralizing antibodies starting at postnatal day P45 prolonged survival, whereas earlier treatment (P16) exacerbated the pathology. These apparently conflicting data can be reconciled by assuming that there is an early period of aortic development in which TGF-β performs a physiological function required for vessel integrity and a later period when excess TGF-β is pathological.

To gain further insight into the contributions of individual TGF-β isoforms to TAA in MFS, we examined the effect of heterozygous deletion of individual TGF-β isoforms (1, 2, and 3) when crossed with mice that have an *Fbn1* mutation yielding a rapidly progressing form of MFS ($Fbn1^{mgR/mgR}$) that includes long bone overgrowth, kyphosis, and dissecting TAA. $Fbn1^{mgR/mgR}$ animals have 50% survival at 80–90 days of age with death caused by aortic ruptures with hemothorax [15]. We found that heterozygous loss of *Tgfb1* or *Tgfb3* had no statistically significant effect on the survival of $Fbn1^{mgR/mgR}$ mice by P70, whereas heterozygous loss of TGF-β2 caused death in over 50% of the $Tgfb2^{+/-}$; $Fbn1^{mgR/mgR}$ animals by P20. Increased mortality was not caused by aortic rupture; rather animals displayed enlarged hearts, aortic roots and aortas, hyperplastic aortic valves, aortic regurgitation, and reduced ejection fraction as well as delayed alveolar septation by P12–16. *Tgfb2* heterozygous mice displayed none of these features. We conclude that the known requirements for TGF-β2 in pre- and early postnatal development of the aorta, heart, and

Author Manuscript Author Manuscript Author Manuscript Author Manuscript

lungs are exacerbated under conditions of limiting amounts of fibrillin1 observed in MFS. This is a further demonstration of the role of fibrillin1 in controlling signaling in the extracellular matrix.

Results

Relative contribution of TGF-β ligand isoforms to survival in the context of MFS

To elucidate a possible role for individual TGF-β isoforms in aortic disease progression in MFS, we generated *Tgfb1*$^{+/-}$*; Fbn1*$^{mgR/mgR}$, *Tgfb2*$^{+/-}$*; Fbn1*$^{mgR/mgR}$ and *Tgfb3*$^{+/-}$*; Fbn1*$^{mgR/mgR}$ mice, reasoning that specific isoform-dependent aortic phenotypes might emerge or be lost under conditions of TGF-β heterozygosity. When survival was monitored until P60-P70 (Fig. 1), more than 90% of control WT, *Tgfb1*$^{+/-}$, *Tgfb2*$^{+/-}$, and *Tgfb3*$^{+/-}$ mice survived. *Fbn1*$^{mgR/mgR}$ mice, which produce only 20–30% of the normal amount of fibrillin1, had 60% survival by P70. The majority of *Fbn1*$^{mgR/mgR}$ deaths (34/38) were associated with hemothorax secondary to aortic rupture, as determined by necropsy (Table 1). Survival of double mutant *Tgfb1*$^{+/-}$*; Fbn1*$^{mgR/mgR}$ and *Tgfb3*$^{+/-}$*; Fbn1*$^{mgR/mgR}$ mice was statistically similar to that of *Fbn1*$^{mgR/mgR}$ mice and no further studies were performed with these genotypes. Conversely, approximately 80% of the *Tgfb2*$^{+/-}$*; Fbn1*$^{mgR/mgR}$ animals died by P20, the time of weaning. There was no evidence of aortic rupture, however, as determined by necropsy (Table 1). The difference in survival between the *Fbn1*$^{mgR/mgR}$ and *Tgfb2*$^{+/-}$*; Fbn1*$^{mgR/mgR}$ mice was striking (p= 0.0001). We also plotted the data from Fig. 1 with respect to sex and found no significant differences (Sup. Fig. 1).

The *Tgfb2*$^{+/-}$*; Fbn1*$^{mgR/mgR}$ survival curve suggested the presence of two cohorts, one that died within the first 20 days and encompassed approximately 75–80% of the animals and one that died over the next 5 weeks that included the remaining 20–25% of the animals. The rate of death of the second cohort resembled that of the *Fbn1*$^{mgR/mgR}$ mice, and six out of six *Tgfb2*$^{+/-}$*; Fbn1*$^{mgR/mgR}$ mice necropsied after P20 had hemothorax, similar to the findings with *Fbn1*$^{mgR/mgR}$ mice.

Aortic dimensions, structure and properties

The primary cause of death in MFS patients and mice is dissection and rupture of the aortic root or ascending aorta, hence we focused initially on the aortas of WT, *Tgfb2*$^{+/-}$, *Fbn1*$^{mgR/mgR}$, and *Tgfb2*$^{+/-}$*; Fbn1*$^{mgR/mgR}$ mice at the gross level (Fig. 2A) and with ultrasound (Table 2). At P12 there were no significant differences in the aortas of WT, *Tgfb2*$^{+/-}$ and *Fbn1*$^{mgR/mgR}$ mice upon examination with both approaches, consistent with prior findings that aortic diameter in *Fbn1*$^{mgR/mgR}$ mice does not differ significantly from WT until P30–45 [14]. By contrast, the aortic roots and ascending aortas of *Tgfb2*$^{+/-}$*; Fbn1*$^{mgR/mgR}$ mice were enlarged compared to WT as measured visually and by ultrasound by P12 (Fig. 2A, Table 2).

The observation that 90% of *Tgfb2*$^{+/-}$*; Fbn1*$^{mgR/mgR}$ mice did not die from aortic rupture was substantiated by histological analysis of the aortas at P12. When stained with Verhoeff-Van Gieson for elastin, the WT aortas had nearly concentric regularly arranged elastic lamellae (Sup. Fig. 2A and B). Aortas from *Tgfb2*$^{+/-}$ mice appeared structurally equivalent

Author Manuscript Author Manuscript Author Manuscript Author Manuscript

to those from WT mice, whereas *Fbn1*$^{mgR/mgR}$ aortas had more breaks in the elastic lamellae compared to WT samples (Sup. Fig. 2C). *Tgfb2*$^{+/-}$*; Fbn1*$^{mgR/mgR}$ aortas, also displayed significant fragmentation of the elastic lamellae (Sup. Fig. 2A, B and C) but appeared to have an increased number of thinner elastic lamellae relative to other genotypes (Sup. Fig. 2A and B). H&E staining, to reveal both cellularity and matrix, of aortic sections indicated no significant differences amongst the four genotypes other than that the *Tgfb2*$^{+/-}$*; Fbn1*$^{mgR/mgR}$ samples may have had somewhat thicker aortic walls (Sup. Fig. 3). We analyzed collagen and proteoglycans in sections of aortas by Picrosirius red and Alcian blue/PAS staining, respectively. We observed no significant differences between the four genotypes at P12 (Sup. Fig. 4). Measurements of aortic diameters of histological sections confirmed the ultrasonic findings that *Tgfb2*$^{+/-}$*; Fbn1*$^{mgR/mgR}$ aortic diameters were significantly larger than those of *Fbn1*$^{mgR/mgR}$ mice (Table 2; Sup. Fig. 2A and E). Interestingly, the values appeared to segregate into two groups, which might represent animals with the two different rates of death.

Aortic microstructure dictates tissue-level properties, which are best quantified by biaxial mechanical testing [16]. Pressure-diameter data collected at P12 for ascending (ATA) and descending (DTA) thoracic aortas, while held fixed at their specimen-specific in vivo axial stretch and pressurized, revealed qualitatively similar structural behaviors across all four genotypes (WT, *Tgfb2*$^{+/-}$, *Fbn1*$^{mgR/mgR}$, and *Tgfb2*$^{+/-}$*; Fbn1*$^{mgR/mgR}$) ordered by increasing diameters for both the ATA (Fig. 3A) and DTA (Fig. 3B). Detailed ex vivo comparisons of multiple geometric and material metrics also revealed qualitatively similar results for the ATA and DTA, though with greater outer diameter, axial stretch, and elastic energy storage in the ATA as expected. Despite the increasing diameter of the ATA across these four genotypes when evaluated at a common distending pressure of 100 mm Hg (Fig. 3C), there was little difference within the ascending segment in either in vivo value of axial stretch or wall thickness except in the *Tgfb2*$^{+/-}$*; Fbn1*$^{mgR/mgR}$ aorta (Fig. 3D, E). Similarly, there was little difference in elastic energy storage capacity across genotypes (Fig. 3F). Relative to WT, wall stress tended to be higher in all three mutants (Fig. 3G) as did circumferential material stiffness (Fig. 3H). Importantly, however, the passive mechanical properties (i.e., in the absence of smooth muscle contractility) tended to be similar between the *Fbn1*$^{mgR/mgR}$ and *Tgfb2*$^{+/-}$*; Fbn1*$^{mgR/mgR}$ mice at this early age (P12), perhaps reflecting a compensatory benefit of additional elastic lamellar structures in the latter despite more breaks. Thus, the lack of marked differences in the structural and mechanical abnormalities in the aorta was consistent with aortopathy but not of early death.

Cardiac size, structure, and function

Hearts of *Fbn1*$^{mgR/mgR}$ mice were larger than those of WT littermate controls (Fig. 2B). At P12, the hearts of *Tgfb2*$^{+/-}$*; Fbn1*$^{mgR/mgR}$ mice were also slightly larger compared to hearts from the other three genotypes (Fig. 2B). Since *Tgfb2*$^{+/-}$*; Fbn1*$^{mgR/mgR}$ mice were somewhat smaller than WT littermates (Fig. 2C), the difference in heart size was more significant when heart weights were normalized to body weights (Fig. 2D). The *Tgfb2*$^{+/-}$*; Fbn1*$^{mgR/mgR}$ hearts appeared to segregate into two cohorts by weight. It is likely (see below) that this more severe phenotype is related to the group of animals that died early.

Author Manuscript Author Manuscript Author Manuscript Author Manuscript

To gain further insight into possible cardiac abnormalities and malfunction, we performed an echocardiographic examination on WT, *Tgfb2*$^{+/-}$, *Fbn1*$^{mgR/mgR}$, and *Tgfb2*$^{+/-}$; *Fbn1*$^{mgR/mgR}$ animals at P12-P14. Cardiac function parameters are summarized in Table 2. As a group, the *Tgfb2*$^{+/-}$; *Fbn1*$^{mgR/mgR}$ mice displayed dilation of the aortic root and aortic regurgitation compared to WT animals. Again, however, *Tgfb2*$^{+/-}$; *Fbn1*$^{mgR/mgR}$ mice could be separated into two groups: one with measurements similar to those of WT or *Tgfb2*$^{+/-}$ mice with respect to fractional shortening and left ventricular diastolic dimensions and one with measurements that were significantly larger. Animals in the group with reduced fractional shortening and left diastolic dimensions also had greater heart weight and aortic diameters.

Cardiac valve structure and function

In order to examine cardiac valve function, we performed echo-Doppler analysis of aortic flow patterns with animals of the four genotypes at P12-P14. Abnormal aortic valve regurgitation, shown in Table 2 as all animals with any abnormal aortic flow or all animals with moderate/severe retrograde aortic flow, was apparent in the subset of compound *Tgfb2*$^{+/-}$; *Fbn1*$^{mgR/mgR}$ mutant mice with enlarged aortas and aortic roots and reduced fractional shortening as demonstrated by diastolic retrograde flow in the ascending and/or descending aorta (Table 2; Fig. 4). These observations are indicative of aortic regurgitation potentially caused by dilation of the aortic root with distortion of the aortic leaflets, or the combination of the two [17]. Again, it is possible that mice with these abnormalities constituted the group of animals with the early death, whereas *Tgfb2*$^{+/-}$; *Fbn1*$^{mgR/mgR}$ mice with minimal aortic changes constituted the group with longer survival. We were able to verify that animals with regurgitation had hearts in the high heart vs body mass group (Fig. 2D).

We found no differences related to sex using groups that had 3 or more mice for each sex. We examined weights, LV dimension, fractional shortening, aortic root diameter, and ascending aortic diameter.

The echo-Doppler results suggesting retrograde blood flow could be explained by abnormal aortic valve leaflets, as both *Fbn1* mutations and TGF-β2 deficiency are associated with defective leaflet formation [18,19]. Therefore, we examined the aortic valves in stained H&E sections from P12 hearts of the four genotypes (Fig. 5). Whereas, WT, *Tgfb2*$^{+/-}$, and *Fbn1*$^{mgR/mgR}$ aortic valves were similar, the *Tgfb2*$^{+/-}$; *Fbn1*$^{mgR/mgR}$ leaflets were significantly enlarged. We also stained sections with Alizarin Red to reveal calcium deposits, as these might impair leaflet function. Aortic leaflets from *Tgfb2*$^{+/-}$; *Fbn1*$^{mgR/mgR}$ animals had more positively stained, dark pigmented regions than leaflets from the other three genotypes (Fig. 5), but it is unclear if this rather limited amount of calcification would impair valve function. Sections of valves from *Tgfb2*$^{+/-}$, *Fbn1*$^{mgR/mgR}$, and *Tgfb2*$^{+/-}$; *Fbn1*$^{mgR/mgR}$ hearts were also stained with Picrosirius Red to reveal collagen (red) and Alcian blue/PAS to reveal mucopoly-saccharides (blue) (Sup. Fig. 5). No striking differences among the genotypes were observed at this early age (P12).

We reasoned that if the hyperplastic leaflets were associated with the early death of the *Tgfb2*$^{+/-}$; *Fbn1*$^{mgR/mgR}$ animals, *Tgfb2*$^{+/-}$; *Fbn1*$^{mgR/mgR}$ mice that survived to P60 should

Author Manuscript Author Manuscript Author Manuscript Author Manuscript

have aortic valve leaflets that resembled WT in both size and calcification. Indeed, as shown in Fig. 5, the surviving *Tgfb2*$^{+/-}$; *Fbn1*$^{mgR/mgR}$ mice had valves that appeared equivalent to those of WT mice. This observation is also consistent with the observation that *Tgfb2*$^{+/-}$; *Fbn1*$^{mgR/mgR}$ mice that died between P45–70 had hemothorax, presumably as a result of their fibrillin1 deficiency (See above).

We also examined the mitral valves and found that the double mutant animals had enlarged leaflets (Sup. Fig. 6). We were unable to measure regurgitation of the mitral valves because of technical limitations of our instrumentation, but given the abnormal leaflets, it is possible that there was altered blood flow.

TGF-β transcription and signaling in aortic tissue

The abnormal aortic phenotypes observed in MFS have been associated with enhanced TGF-β expression and signaling [2,20]. To determine if TGF-β signaling was altered amongst the four genotypes, we used immunoblotting of aortic extracts to examine signaling through the canonical Smad pathway, by quantifying pSmad3 levels, and the non-canonical pathway, by measuring pErk levels. There was an increase in TGF-β signaling through both pathways in *Tgfb2*$^{+/-}$ aortas compared to WT tissue and an equal or even greater degree of signaling in *Tgfb2*$^{+/-}$; *Fbn1*$^{mgR/mgR}$ aortic extracts (Fig. 6A). To establish if the loss of one *Tgfb2* allele altered cytokine expression levels, we measured the transcription of *Tgfb2,* as well as *Tgfb1* and *Tgfb3,* in extracts from aortas of WT, *Tgfb2*$^{+/-}$, *Fbn1*$^{mgR/mgR}$, and *Tgfb2*$^{+/-}$; *Fbn1*$^{mgR/mgR}$ mice. *Tgfb1* and *Tgfb3* expression remained essentially the same in four genotypes, and *Tgfb2* expression was significantly lower in the aortas from *Tgfb2*$^{+/-}$ and *Tgfb2*$^{+/-}$; *Fbn1*$^{mgR/mgR}$ mice, as expected (Fig. 6B).

A recent report described focal activation of TGF-β signaling in aortopathy [21]. Therefore, the lack of differences in the transcript patterns illustrated in Fig. 6B could have resulted from analyzing the entire ascending aorta plus valves, which would have averaged results and possibly obscured regional differences. Indeed, the major difference that we observed was in the aortic valves that comprise a minor amount of the material analyzed in Fig. 6. Therefore, we used immunohistochemistry to measure the amount and distribution of pErk1/2 and immunofluorescence to measure pSmad2 levels and distribution in aortic valves. The results (Sup. Fig. 7A and B) indicate that the level of signaling for both molecules is highest for *Tgfb2*$^{+/-}$; *Fbn1*$^{mgR/mgR}$ animals followed by *Tgfb2*$^{+/-}$, and *Fbn1*$^{mgR/mgR}$ animals, both of which were higher than the WT samples. The staining patterns are consistent with the immune blotting illustrated in Fig. 6A and do not appear to reveal specific regional differences among the genotypes that might account for the lack of transcript differences.

Morphometric analysis of lung parenchyma

In addition to aortic pathology, many MFS patients display abnormal lung function and overt pulmonary manifestations, including emphysema, hyperinflation, pneumothorax, and diffusion impairment, as well as moderate to severe rib cage deformities [22]. The role of TGF-β in lung development is well established and dysregulated TGF-β activation appears to impair alveolar septation in *Fbn1*$^{mgR/mgR}$ mice during postnatal lung development [5].

Author Manuscript Author Manuscript Author Manuscript Author Manuscript

To ascertain whether reduced TGF-β2 alters the postnatal lung phenotype of *Tgfb2*$^{+/-}$; *Fbn1*$^{mgR/mgR}$ mice as well as examining the lungs for indications of congestive heart failure, we evaluated the lungs of WT, *Tgfb2*$^{+/-}$, *Fbn1*$^{mgR/mgR}$, and *Tgfb2*$^{+/-}$; *Fbn1*$^{mgR/mgR}$ mice at P12 (Fig. 7). We assessed morphology and morphometry on H&E-stained cross-sections of lungs that were fixed at the same inflation pressure. WT and *Tgfb2*$^{+/-}$ lungs show normal appearing lung parenchyma containing alveoli and alveolar ducts, whereas *Fbn1*$^{mgR/mgR}$ lungs exhibit enlarged alveolar airspaces and mild to moderate septation anomalies. In contrast, *Tgfb2*$^{+/-}$; *Fbn1*$^{mgR/mgR}$ lungs exhibit large deformed alveolar airspaces with rare secondary septa. To quantify the differences, we measured two lung morphometric parameters: the mean linear intercept (MLI) and tissue-alveolar (T/A) ratio (Fig. 7B and C). Slightly increased MLI and decreased T/A ratios were seen in *Tgfb2*$^{+/-}$ lungs compared to WT lungs. These differences were accentuated in *Fbn1*$^{mgR/mgR}$ lungs when compared to WT and *Tgfb2*$^{+/-}$ lungs and were even more severe in *Tgfb2*$^{+/-}$; *Fbn1*$^{mgR/mgR}$ lungs, corroborating the morphologic abnormalities we observed. There was almost a complete absence of secondary septa consistent with developmental arrest at the early alveolar stage.

We also weighed the right and left lungs from animals of the four genotypes and compared them after normalization to body weight. The results (Sup. Fig. 6) showed no significant differences in weights. The lack of a difference in lung weight suggests that the *Tgfb2*$^{+/-}$; *Fbn1*$^{mgR/mgR}$ animals had no significant pulmonary edema.

Discussion

The initial goal of these experiments was to identify which TGF-β isoform contributed to the aortopathy in mice with MFS. However, although selected published data might suggest a diminution of the MFS phenotype upon TGF-β2 reduction [5,7], we observed that in MFS mice loss of a single allele of *Tgfb2,* but not *Tgfb1* or *Tgfb3*, resulted in earlier death, with 80% of the double mutant mice dying by P20 compared to 50% death in MFS alone mice by P70. These results are consistent with other reports (see below) that the genetic reduction of TGF-β2 expression or signaling can result in enhanced phenotypes. Unexpectedly, this increased mortality was not the consequence of thoracic aortic dissection and rupture. Therefore, we cannot conclude which TGF-β isoform is associated with the lethal vascular phenotypes in MFS.

Our results may, however, help explain the observed dimorphic effect of TGF-β inhibition with respect to aneurysm development in MFS. That is, aortopathy is increased by early elimination of TGF-β signaling either by conditional *Tgfbr2* gene deletion (at P21 or P28) or by neutralizing TGF-β antibody treatment (starting at P16) in MFS animals, whereas the inhibition of TGF-β using pharmacological or antibody-based approaches yields a favorable effect when initiated at later times including P45 [10,11,13,14]. These apparently opposite effects may reflect the consequences of loss of the beneficial early contributions of TGF-β2 to aortic development and maturation versus later abrogation of the pathological consequences of aberrant TGF-β activity after vessel maturation.

Our findings in the *Tgfb2*$^{+/-}$ aorta at P12 are consistent with many biomechanical properties evolving with increasing age into maturity. To gain further insight into the TGF-β2 related

Author Manuscript Author Manuscript Author Manuscript Author Manuscript

contributions to early death, we focused on cardiovascular structure and function at postnatal day 12 given the 50% mortality of the *Tgfb2*$^{+/-}$; *Fbn1*$^{mgR/mgR}$ mice by P20. Importantly, others have shown that the elastic lamellar structures within the aorta tend not to be mature biomechanically (i.e., fully functional as elastic energy storage structures) until about P20, whereas overall the aorta is not biomechanically mature until about P56 due to continued collagen deposition and organization [16]. The most characteristic biomechanical feature of the aneurysmal thoracic aorta is an increased circumferential material stiffness, though reduced elastic energy storage is likewise common [23,24]. We show that circumferential material stiffness was higher in the ascending aortas in all three mutant models (*Tgfb2*$^{+/-}$, *Fbn1*$^{mgR/mgR}$, and *Tgfb2*$^{+/-}$; *Fbn1*$^{mgR/mgR}$) relative to WT even at this early postnatal stage, before the development of an aneurysm (>50% increase in diameter). This suggests that an altered microstructure affecting biomechanical function manifests prior to imaging-based detection of aneurysm. Finally, although wall stress was higher than normal in the mutant mice, these values (< 80 kPa) were significantly less than the values (> 200 kPa) at which the mature aorta tends to rupture in *Fbn1*$^{mgR/mgR}$ mice. It appears, therefore, that the lack of aortic rupture at or before P20 was likely due to the modest structural and functional changes at the lower blood pressures characteristic of early postnatal development, and thus low wall stress. Although we focused on the biomechanical properties of the immature *Tgfb2*$^{+/-}$; *Fbn1*$^{mgR/mgR}$ aorta, a recent study compared biomechanical properties in mature (4–5-month-old) WT, *Tgfb1*$^{+/-}$, *Tgfb2*$^{+/-}$, and *Tgfb3*$^{+/-}$ mice [25]. The authors reported no aortopathy, though the *Tgfb2*$^{+/-}$ aortas showed the greatest differences from WT with increased wall thickness, decreased wall stress, decreased stiffness, and decreased energy storage. We did not assess vasoactive properties since they are lowest at P12 [16], which renders it difficult to assess endothelial-mediated vasodilation. Altered endothelial cell function may have contributed to the differential mechanical properties, but this was not explored given the absence of aortic dissection or rupture phenotype at P12.

The precise cause of death of these *Tgfb2*$^{+/-}$; *Fbn1*$^{mgR/mgR}$ mice remains unclear. Although *Tgfb2*$^{+/-}$; *Fbn1*$^{mgR/mgR}$ mice displayed enlarged aortic roots and ascending aortas when compared to the other genotypes, it is unlikely that these abnormalities led to their early demise as none of the mice examined that died prior to P20 had hemothorax. As discussed above, biaxial biomechanical phenotyping of the ascending aorta across the four genotypes of interest revealed only modest differences between *Fbn1*$^{mgR/mgR}$ and *Tgfb2*$^{+/-}$; *Fbn1*$^{mgR/mgR}$ mice, perhaps due to the increased number of elastic lamellar structures off-setting an increased number of elastic breaks in the double mutant mice. *Tgfb2*$^{+/-}$; *Fbn1*$^{mgR/mgR}$ mice also had aortic regurgitation and reduced ejection fractions, as well as larger hearts and abnormal aortic valve leaflets.

Dilation of the heart with significant regurgitation and decreased ejection fraction might lead to sudden arrhythmic death. Individuals with MFS can display myocardial impairment independent of valvular abnormalities and such cardiomyopathy may lead to or be associated with ventricular arrhythmias [26–28]. Animals that had abnormal heart function also appeared to have increased heart weight, increased aortic diameter, and hyperplastic aortic leaflets. These features suggested left-ventricular heart failure as a potential cause of death, but one of the common consequences, pulmonary edema, was not found upon histological examination of the lungs. However, given our findings of significantly impaired

Author Manuscript Author Manuscript Author Manuscript Author Manuscript

postnatal lung development, it is possible that abnormal lung function and gas exchange might have added to the cardiac dysfunction in the early death of these mice.

It should be noted that we do not understand why certain *Tgfb2*$^{+/-}$; *Fbn1*$^{mgR/mgR}$ mice did not develop the aortic valve pathologies observed with those animals that died early. Whether this is an effect of modifier genes in the mixed background we used or epigenetic changes remains to be determined.

Our basic aortic structural and survival results can be compared with other studies that used double mutants to investigate effects of TGF-β signaling perturbation in MFS mice. It has been reported that *Smad4*$^{+/-}$; *Fbn1*$^{C1041G/+}$ mice have significantly increased aortic disease severity [29], that *Tgfb2*$^{+/-}$; *Fbn1*$^{C1041G/+}$ mice have increased aortic root dilatation [30], and that *Fbn1*$^{C1041G/+}$; *Tgfbr1*$^{f/f}$ Tmx mice exhibit a significantly worse phenotype with hemo-thorax [10]. These previous results are all consistent with our findings of dysregulated TGF-β signaling synergizing with fibrillin1 mutations. It should be stressed that these earlier studies used *Fbn1*$^{C1041G/+}$ mice with mild phenotype that develops over the first year of life [31], whereas we used hypomorphic *Fbn1*$^{mgR/mgR}$ mice that exhibit a much more accelerated and severe phenotype. The one exception to the general finding that disturbed TGF-β signaling results in an abnormal aortic phenotype is *Ltbp3*$^{-/-}$; *Fbn1*$^{mgR/mgR}$ mice in which the MFS related aortopathy improves [32,33], though the underlying mechanism for this observation is not understood.

An interesting question is whether secondary pathological mutations would enhance the phenotype in humans with *Fbn1* mutations that do not reduce total fibrillin1 to the extent observed in mgR mice.

TGFB2 haploinsufficiency has been reported to result in aneurysms and dissection associated with increased TGF-β signaling in humans [30,34]. *Tgfb2* deficiency was also described to exacerbate both TGF-β signaling and the aortic phenotype in *Fbn1*$^{C1041G/+}$ mice, which have a slowly progressing form of MFS with aneurysms apparent only after 2–4 months. but this did not appear to result in enhanced death [30], unlike our observations. Lindsay and colleagues also reported roughly equivalent levels of expression of *Tgfb2* and *Tgfb3,* and a slight increase in *Tgfb1* expression in the MFS mice heterozygous for *Tgfb2*. The lack of a lethal phenotype in this earlier study may reflect the fact that the *Fbn1*$^{C1041G/+}$ mutation yields a slowly progressing form of MFS and ruptures are rarely observed and only in older mice [35]. Interestingly, as we found enhanced TGF-β signaling without any significant increases in *Tgfb* expression, it is possible that the increased TGF-β signaling is due to dysregulated control of latent TGF-β activation in the presence of limiting fibrillin1.

Other studies have demonstrated a role for TGF-β2 in the early development of the heart valves and associated vessels as well as lungs [18,36–39]. Therefore, it is not surprising that we observed structural and functional abnormalities in the aorta, heart, and lungs. *Tgfb2* haploinsufficiency is associated with a spectrum of connective tissue alterations in humans but has not been reported to result in early death [30,34,40]; i. e., there is only one publication describing sudden death in an individual with a *Tgfb2* mutation, but thus far this is an isolated case [41]. *Tgfb2* haploinsufficiency has similarly not been associated

Author Manuscript Author Manuscript Author Manuscript Author Manuscript

with early death in mice, consistent with our findings. Lindsay and colleagues did report the presence of aneurysms and associated changes in the media in *Tgfb2*$^{+/-}$mice at 8 months of age [30]. But, as we show here, only when the loss of TGF-β2 is combined with the diminution of fibrillin1 do the animals die early. The precise reason for this synergistic effect remains to be determined. An open question is, what is the cellular source of the TGF-β associated with aortic aneurysms and rupture? Several possibilities exist including the smooth muscle cells of the media, fibroblasts in the adventitia, or infiltrating cells such as leukocytes. Another unresolved question is whether the contributing TGF-β in aneurysm progression and dissection in mature mice is TGF-β1, 2, or 3. Future experiments will be needed to address these issues.

Experimental procedures

Mice

Tgfb1$^{+/-}$, *Tgfb2*$^{+/-}$ and *Tgfb3*$^{+/-}$ mice were provided by Dr. Thomas Doetschman (University of Arizona, Tucson, USA) [38,42,43]. *Fbn1*$^{mgR/mgR}$ mice were a gift from Dr. Francesco Ramirez (Mount Sinai School of Medicine, New York, USA) [15]. Mice were maintained on a mixed C57BL/6; Sv129; SW genetic background. Littermates were used for all experiments, and animals were euthanized by CO_2 asphyxiation. All experiments used mixed population of males and females and were conducted using a protocol approved by Institutional Animal Care and Use Committee (IACUC) at the New York University Langone Medical Center.

Echocardiography

Transthoracic echocardiography was performed in standard fashion as described previously [32,44], using a Fujifilm Vevo 770 Visual Sonics ultrasound system with a 40-MHz center frequency transducer [44]. Mice were anesthetized in an induction chamber with 1% isoflurane mixed with room air via a nose cone and placed on the imaging platform in the supine position with isoflurane maintained via the anesthetic nose cone. Core (rectal) temperature was maintained at 37 ± 1 °C. Analyses included left ventricle diastolic dimensions, fractional shortening, and aortic root and ascending aortic diameters (in systole). Basic cardiac rhythm was monitored by electrocardiographic limb leads on the warming pad on which the mouse lay and was simultaneously displayed with echocardiographic images. All echocardiographic measurements were performed in triplicate, averaged, and scored without knowledge of genotype.

Aortic mechanics

Following euthanasia at P12 of mice of all four key genotypes of interest (WT, *Tgfb2*$^{+/-}$, *Fbn1*$^{mgR/mgR}$, *Tgfb2*$^{+/-}$; *Fbn1*$^{mgR/mgR}$), the thoracic aorta was excised by gentle dissection from the aortic root to the diaphragm and placed in a chilled physiologic solution for overnight shipment and biomechanical phenotyping. We have shown previously that delaying such testing overnight adversely affects the vasoactive function but not the passive mechanical properties [45]. Loose peri−adventitial tissue was removed and the ascending (ATA) and descending (DTA) segments of the thoracic aorta were cannulated separately with glass micro-pipets and placed within a custom biaxial testing system [46] in Hanks'

Author Manuscript Author Manuscript Author Manuscript Author Manuscript

Balanced Salt Solution at room temperature. Following equilibration and preconditioning, the vessels were subjected to a standardized loading protocol to quantify the passive mechanical properties [47]. Specifically, each vessel was subjected to 7 biaxial protocols resulting in >700 pressure, diameter, axial force, and axial extension measurements per vessel (i. e. >2800 data points per vessel): cyclic pressurization from 10 to 80 mm Hg at three fixed values of axial stretch ($0{:}95\lambda_{z;\mathrm{iv}}$, $1{:}00\lambda_{z;\mathrm{iv}}$, and $1{:}05\lambda_{z;\mathrm{iv}}$, where $\lambda_{z;\mathrm{iv}}$ is the energetically preferred in vivo stretch) and cyclic axial loading from $f = 0$ to $f = f_{\max}$ at four fixed pressures (10, 40, 60, and 80 mmHg), where $f_{\max}$ corresponds to the maximum specimen-specific force reached during the pressurization protocol at axial stretch $1{:}05l_{z;\mathrm{iv}}$. The unloading data from each second cycle of loading were used to determine best-fit values of the material parameters in a validated nonlinear constitutive relation from which one can compute biaxial stresses, stiffnesses, stored energy, etc. which collectively define passive mechanical properties [48].

Cardiovascular tissue histology and visualization of tissue structures

Hearts from mice euthanized at P12 were perfused with 1xPBS and the ascending aorta and aortic valve plus heart were harvested and fixed in 10% PBS/formalin (vol/vol) for 48 h. Samples were dehydrated and embedded in paraffin. Sections (5 μm) of paraffin embedded ascending aortas/aortic valves or hearts were stained with Hematoxylin & Eosin (H&E). Elastin and collagen were visualized by Verhoeff-Van Gieson and Picrosirius red staining, respectively. Aortic leaflet calcification was analyzed by Alizarin red staining and Proteoglycan was examined by Alcian blue/PAS stain. Images were digitally captured using a whole slide digital scanner (Leica SCN 400) and Leica SlidePath software. Two individuals, blinded to the genotype, manually counted the number of elastin breaks (free ends) along the elastic lamellae in a transverse section of the ascending aorta. This approach was applied to two equally distanced sections along the vessel length of each mouse. Aortas were imaged under a stereo-microscope for diameter measurement using NIH Image J software; 10 measurements of the aortic diameter were taken at equal intervals of the ascending aorta starting at the root and averaged.

Lung histology and morphometry

Lung harvest, processing, and evaluation was performed as described with minor modifications [49]. After euthanasia with CO_2, the lungs were inflated through the trachea with 4% paraformaldehyde at a pressure 25 cm H_2O for 15 min. Lungs were fixed for 24 h, processed, and embedded in paraffin. H&E-stained sections (5 μm) were analyzed without knowledge of the genotype of the animals. Random fields (~10 per lung) of the alveolar compartments were considered for the analysis from a whole slide digital scanned image (Leica SCN 400). For the quantitative assessment of alveolar airspaces, the mean linear intercept (MLI) was used as a measure of alveolar airspace. Images were analyzed in batches by ImageJ software using a custom macro tool to overlay lines and measure their lengths. The same macro tool was used to perform tissue/alveolar (T/A) airspace ratio measurements, wherein the quantity of alveolar tissue area relative to the area of the alveolar spaces was ascertained. An R-script was used in the software R Studio to aggregate all text files of MLI data generated from images into a single excel document for each sample, yielding an average MLI calculated for those generated for each sample.

Author Manuscript Author Manuscript Author Manuscript Author Manuscript

Antibodies

Antibodies used for immunoblotting were rabbit polyclonal anti-pSmad3 from Abcam (Ab51451), rabbit monoclonal anti-pERK1/2 from Cell Signaling (4370), and mouse anti-G3PDH (clone 6C5) from Santa Cruz (sc-32233).

Immunoblotting

Immunoblotting was performed as described by Zilberberg et al. [32].

Immunofluorescence

For detection of pSmad2, Paraffin embedded 5 μm cross-sections of aortic valves were deparaffinized and incubated with Antigen retrieval solution (Agilent Dako #S238964–2) overnight at 4 °C followed by boiling in the antigen retrieval solution for 5 min. Sections were then permeabilized with PBS containing 0.1% Triton X-100 and 0.3 M glycine for 20 min, incubated in Fc receptor blocker (Innovex biosciences # NB309–5S) for 20 min and followed by treatment with Background Buster (Innovex biosciences # NB306–7) for 20 min [21]. Primary antibody was diluted in PBS containing 0.1% Triton X-100. Samples were incubated overnight in primary antibody, anti-pSmad2 (ThermoFisher Scientific #44–244 G) at a dilution of 1:100 at 4 °C. The next day, samples were washed 3 times in PBS containing 0.1% Triton X-100 at the interval of 5 min and incubated in secondary antibody, goat anti-Rabbit Alexa 555 (Invitrogen #A-21,428) at a dilution of 1:200 at room temperature. Sample were washes 3 times at intervals of 5 min and mounted with ProLong™ Gold Antifade Mountant with DAPI (Invitrogen #P36931). Images were acquired with a Zeiss LSM760 confocal microscope.

Immunohistochemistry

Immunohistochemical staining of aortic valves was performed with a Leica BondRX automated stainer, according to the manufacturer instructions. In brief, tissues for immunostaining underwent deparaffinization online followed by epitope retrieval for 20 min at 100°C with Leica Biosystems ER1 solution (pH6,0 #AR9961) and endogenous peroxidase activity blocking with H_2O_2. Sections were incubated with primary antibodies against pERK (Cell Signaling Technologies # 4376S; clone 20G11) at a dilution of 1:300 for 30 min at room temperature. Primary antibodies were detected with anti-rabbit HRP-conjugated polymer and 3,3′-diaminobenzidine (DAB) substrate provided in the Leica BOND Polymer Refine Detection System (#DS9800). Following counter-staining with haematoxylin, slides were scanned at 20X on a Hamamatzu Nanozoomer 2.0HT whole slide scanner and the image files uploaded to the NYUGSoM's OMERO Plus image data management system (Glencoe Software).

Gene expression analysis

Total RNA from ascending aortas was isolated as per protocol using the RNeasy Fibrous Tissue Mini Kit (Qiagen). 1 μg RNA from each sample was transcribed into cDNA using an iScript cDNA synthesis kit (Biorad) following the manufacturer's instructions. Relative expression of target genes was evaluated by quantitative real-time PCR (qPCR) using SYBR green Supermix (Applied Biosystems) on an iCycler Thermal Cycler (Bio-Rad)

Author Manuscript Author Manuscript Author Manuscript Author Manuscript

using specific primers (Sequences are provided in Table S1). Relative mRNA expression was calculated using the AACt method and each target transcript expression was quantified relative to the reference gene, GAPDH. The annealing temperature was 60 °C.

Statistics

Statistical analysis for all graphs, including Kaplan-Meier survival curves, was performed using GraphPad Prism 9.0 (GraphPad Software, Inc. La Jolla, CA). Kaplan-Meier survival curve statistics were analyzed using log-rank (Mantel-Cox) test. All values are expressed as mean ± SD in the graphs except for Fig. 3 in which values are expressed as mean ± SEM. Statistical difference between two groups was determined using unpaired two-tailed student's *t*-test. $p < 0.05$ was considered as significant value. Analysis between multiple groups was performed using one-way ANOVA assuming significance at $p<0.05$. Non-parametric data analysis for P12 lungs MLI and T/A ratio was analyzed using Kruskal-Wallis test to analyze statistical significance, considering $p<0.05$ as significant. * = $p<0.05$, ** = $p<0.01$, *** = $p<0.005$, **** = $p<0.001$.

Supplementary Material

Refer to Web version on PubMed Central for supplementary material.

Acknowledgements

We acknowledge the use of the New York University Langone Medical Center (NYUMC) Histopathology and Transgenic Mouse Cores supported by NYUMC Cancer Center Grant P30CA016087, National Institutes of Health. This work was also supported, in part, by and was performed at the Pre-clinical Imaging laboratory supported by the Laura and Isaac Perlmutter Cancer Center Support Grant NCI SP30CA016087 and NIBIB Biomedical Technology Resource Center Grant NIH P41 E8017183. We thank Dr. Santosh Kumar for technical assistance, Dr. Karan Singh for helpful suggestions, Dr. Rashmi Mishra for input in the western blot quantification and Esme Zediker for assistance in genotyping of mice.

Funding

This work was supported by a grant P01 HL134605 from the National Heart, Lung, and Blood Institute to JDH and DBR and grants from NHLBI R56-HL151700, the Stony Wold-Herbert Foundation, and the Will-Rogers Foundation to MCK.

Data availability

Data will be made available upon reasonable request.

Abbreviations:

MFS	Marfan Syndrome
TAA	Thoracic Aortic Aneurysm
AR	Aortic Regurgitation
LTBPs	Latent TGF-β Binding Proteins

Author Manuscript Author Manuscript Author Manuscript Author Manuscript

References

[1]. Ikushima H, Miyazono K, Cellular context-dependent “colors” of transforming growth factor-beta signaling, Cancer Sci 101 (2010) 306–312. [PubMed: 20067465]

[2]. MacFarlane EG, Haupt J, Dietz HC, Shore EM, TGF-beta Family Signaling in Connective Tissue and Skeletal Diseases, Cold Spring Harb. Perspect. Biol 9 (2017).

[3]. Wheeler JB, Ikonomidis JS, Jones JA, Connective tissue disorders and cardiovascular complications: the indomitable role of transforming growth factor-beta signaling, Adv. Exp. Med. Biol 802 (2014) 107–127. [PubMed: 24443024]

[4]. Wheeler JB, Ikonomidis JS, Jones JA, Connective Tissue Disorders and Cardiovascular Complications: the Indomitable Role of Transforming Growth Factor-beta Signaling, Adv. Exp. Med. Biol 1348 (2021) 161–184. [PubMed: 34807419]

[5]. Neptune ER, Frischmeyer PA, Arking DE, Myers L, Bunton TE, Gayraud B, Ramirez F, Sakai LY, Dietz HC, Dysregulation of TGF-βeta activation contributes to pathogenesis in Marfan syndrome, Nat. Genet 33 (2003) 407–411. [PubMed: 12598898]

[6]. Ramirez F, Dietz HC, Marfan syndrome: from molecular pathogenesis to clinical treatment, Curr. Opin. Genet. Dev 17 (2007) 252–258. [PubMed: 17467262]

[7]. Habashi JP, Judge DP, Holm TM, Cohn RD, Loeys BL, Cooper TK, Myers L, Klein EC, Liu G, Calvi C, Podowski M, Neptune ER, Halushka MK, Bedja D, Gabrielson K, Rifkin DB, Carta L, Ramirez F, Huso DL, Dietz HC, Losartan, an AT1 antagonist, prevents aortic aneurysm in a mouse model of Marfan syndrome, Science 312 (2006) 117–121. [PubMed: 16601194]

[8]. Pitcher A, Spata E, Emberson J, Davies K, Halls H, Holland L, Wilson K, Reith C, Child AH, Clayton T, Dodd M, Flather M, Jin XY, Sandor G, Groenink M, Mulder B, De Backer J, Evangelista A, Forteza A, Teixido-Tura G, Boileau C, Jondeau G, Milleron O, Lacro RV, Sleeper LA, Chiu HH, Wu MH, Neubauer S, Watkins H, Dietz H, Baigent C, Marfan C, Treatment Trialists, Angiotensin receptor blockers and beta blockers in Marfan syndrome: an individual patient data meta-analysis of randomised trials, Lancet 400 (2022) 822–831. [PubMed: 36049495]

[9]. Bento JR, Meester J, Luyckx I, Peeters S, Verstraeten A, Loeys B, The genetics and typical traits of thoracic aortic aneurysm and dissection, Annu. Rev. Genomics Hum. Genet 23 (2022) 223–253. [PubMed: 36044906]

[10]. Li W, Li Q, Jiao Y, Qin L, Ali R, Zhou J, Ferruzzi J, Kim RW, Geirsson A, Dietz HC, Offermanns S, Humphrey JD, Tellides G, Tgfbr2 disruption in postnatal smooth muscle impairs aortic wall homeostasis, J. Clin. Invest 124 (2014) 755–767. [PubMed: 24401272]

[11]. Hu JH, Wei H, Jaffe M, Airhart N, Du L, Angelov SN, Yan J, Allen JK, Kang I, Wight TN, Fox K, Smith A, Enstrom R, Dichek DA, Postnatal Deletion of the Type II Transforming Growth Factor-beta Receptor in Smooth Muscle Cells Causes Severe Aortopathy in Mice, Arterioscler. Thromb. Vasc. Biol 35 (2015) 2647–2656. [PubMed: 26494233]

[12]. Wei H, Hu JH, Angelov SN, Fox K, Yan J, Enstrom R, Smith A, Dichek DA, Aortopathy in a Mouse Model of Marfan Syndrome Is Not Mediated by Altered Transforming Growth Factor beta Signaling, J. Am. Heart Assoc 6 (2017).

[13]. Tellides G, Further Evidence Supporting a Protective Role of Transforming Growth Factor-beta (TGFbeta) in Aortic Aneurysm and Dissection, Arterioscler. Thromb. Vasc. Biol 37 (2017) 1983–1986. [PubMed: 29070536]

[14]. Cook JR, Clayton NP, Carta L, Galatioto J, Chiu E, Smaldone S, Nelson CA, Cheng SH, Wentworth BM, Ramirez F, Dimorphic effects of transforming growth factor-beta signaling during aortic aneurysm progression in mice suggest a combinatorial therapy for Marfan syndrome, Arterioscler. Thromb. Vasc. Biol 35 (2015) 911–917. [PubMed: 25614286]

[15]. Pereira L, Lee SY, Gayraud B, Andrikopoulos K, Shapiro SD, Bunton T, Biery NJ, Dietz HC, Sakai LY, Ramirez F, Pathogenetic sequence for aneurysm revealed in mice underexpressing fibrillin-1, Proc. Natl. Acad. Sci. U S A, 96 (1999) 3819–3823. [PubMed: 10097121]

[16]. Murtada SI, Kawamura Y, Li G, Schwartz MA, Tellides G, Humphrey JD, Developmental origins of mechanical homeostasis in the aorta, Dev. Dyn 250 (2021) 629–639. [PubMed: 33341996]

Author Manuscript Author Manuscript Author Manuscript Author Manuscript

[17]. Maurer MS, Obesity and the risk of heart failure, N. Engl. J. Med 347 (2002) 1887–1889 author reply 1887–1889.

[18]. Azhar M, Brown K, Gard C, Chen H, Rajan S, Elliott DA, Stevens MV, Camenisch TD, Conway SJ, Doetschman T, Transforming growth factor Beta2 is required for valve remodeling during heart development, Dev. Dyn 240 (2011) 2127–2141. [PubMed: 21780244]

[19]. Pepe G, Nistri S, Giusti B, Sticchi E, Attanasio M, Porciani C, Abbate R, Bonow RO, Yacoub M, Gensini GF, Identification of fibrillin 1 gene mutations in patients with bicuspid aortic valve (BAV) without Marfan syndrome, BMC Med. Genet 15 (2014) 23. [PubMed: 24564502]

[20]. Lindsay ME, Dietz HC, The genetic basis of aortic aneurysm, Cold Spring Harb. Perspect. Med 4 (2014) a015909. [PubMed: 25183854]

[21]. MacFarlane EG, Parker SJ, Shin JY, Kang BE, Ziegler SG, Creamer TJ, Bagirzadeh R, Bedja D, Chen Y, Calderon JF, Weissler K, Frischmeyer-Guerrerio PA, Lindsay ME, Habashi JP, Dietz HC, Lineage-specific events underlie aortic root aneurysm pathogenesis in Loeys-Dietz syndrome, J. Clin. Invest 129 (2019) 659–675. [PubMed: 30614814]

[22]. Corsico AG, Grosso A, Tripon B, Albicini F, Gini E, Mazzetta A, Di Vincenzo EM, Agnesi ME, Tsana Tegomo E, Ronzoni V, Arbustini E, Cerveri I, Pulmonary involvement in patients with Marfan Syndrome, Panminerva Med 56 (2014) 177–182. [PubMed: 24994580]

[23]. Bellini C, Bersi MR, Caulk AW, Ferruzzi J, Milewicz DM, Ramirez F, Rifkin DB, Tellides G, Yanagisawa H, Humphrey JD, Comparison of 10 murine models reveals a distinct biomechanical phenotype in thoracic aortic aneurysms, J. R. Soc. Interface 14 (2017).

[24]. Cavinato C, Chen M, Weiss D, Ruiz-Rodriguez MJ, Schwartz MA, Humphrey JD, Progressive Microstructural Deterioration Dictates Evolving Biomechanical Dysfunction in the Marfan Aorta, Front Cardiovasc. Med 8 (2021) 800730. [PubMed: 34977201]

[25]. Lane BA, Chakrabarti M, Ferruzzi J, Azhar M, Eberth JF, Mechanics of ascending aortas from TGFbeta-1, −2, −3 haploinsufficient mice and elastase-induced aortopathy, J. Biomech 125 (2021) 110543. [PubMed: 34174532]

[26]. Andersen NH, Groth KA, Berglund A, Hove H, Gravholt CH, Stochholm K, Non-aortic cardiovascular disease in Marfan syndrome: a nationwide epidemiological study, Clin. Res. Cardiol 110 (2021) 1106–1115. [PubMed: 33885997]

[27]. Aydin A, Adsay BA, Sheikhzadeh S, Keyser B, Rybczynski M, Sondermann C, Detter C, Steven D, Robinson PN, Berger J, Schmidtke J, Blankenberg S, Willems S, von Kodolitsch Y, Hoffmann BA, Observational cohort study of ventricular arrhythmia in adults with Marfan syndrome caused by FBN1 mutations, PLoS ONE 8 (2013) e81281. [PubMed: 24349050]

[28]. Demolder A, Bianco L, Caruana M, Cervi E, Evangelista A, Jondeau G, Buttigieg LL, Lopez-Sainz A, Delmas EM, Pini A, Sabate-Rotes A, Szocs K, Tchitchinadze M, Teixido-Tura G, von Kodolitsch Y, Muino-Mosquera L, De Backer J, Arrhythmia and impaired myocardial function in heritable thoracic aortic disease: an international retrospective cohort study, Eur. J. Med. Genet 65 (2022) 104503.

[29]. Holm TM, Habashi JP, Doyle JJ, Bedja D, Chen Y, van Erp C, Lindsay ME, Kim D, Schoenhoff F, Cohn RD, Loeys BL, Thomas CJ, Patnaik S, Marugan JJ, Judge DP, Dietz HC, Noncanonical TGFbeta signaling contributes to aortic aneurysm progression in Marfan syndrome mice, Science 332 (2011) 358–361. [PubMed: 21493862]

[30]. Lindsay ME, Schepers D, Bolar NA, Doyle JJ, Gallo E, Fert-Bober J, Kempers MJ, Fishman EK, Chen Y, Myers L, Bjeda D, Oswald G, Elias AF, Levy HP, Anderlid BM, Yang MH, Bongers EM, Timmermans J, Braverman AC, Canham N, Mortier GR, Brunner HG, Byers PH, Van Eyk J, Van Laer L, Dietz HC, Loeys BL, Loss-of-function mutations in TGFB2 cause a syndromic presentation of thoracic aortic aneurysm, Nat. Genet 44 (2012) 922–927. [PubMed: 22772368]

[31]. Gharraee N, Sun Y, Swisher JA, Lessner SM, Age and sex dependency of thoracic aortopathy in a mouse model of Marfan syndrome, Am. J. Physiol. Heart Circ. Physiol 322 (2022) H44–H56. [PubMed: 34714692]

[32]. Zilberberg L, Phoon CK, Robertson I, Dabovic B, Ramirez F, Rifkin DB, Genetic analysis of the contribution of LTBP-3 to thoracic aneurysm in Marfan syndrome, Proc. Natl. Acad. Sci. U. S. A 112 (2015) 14012–14017. [PubMed: 26494287]

Author Manuscript Author Manuscript Author Manuscript Author Manuscript

[33]. Korneva A, Zilberberg L, Rifkin DB, Humphrey JD, Bellini C, Absence of LTBP-3 attenuates the aneurysmal phenotype but not spinal effects on the aorta in Marfan syndrome, Biomech. Model. Mechanobiol 18 (2019) 261–273. [PubMed: 30306291]

[34]. Boileau C, Guo DC, Hanna N, Regalado ES, Detaint D, Gong L, Varret M, Prakash SK, Li AH, d'Indy H, Braverman AC, Grandchamp B, Kwartler CS, Gouya L, Santos-Cortez RL, Abifadel M, Leal SM, Muti C, Shendure J, Gross MS, Rieder MJ, Vahanian A, Nickerson DA, Michel JB, National Heart L, Blood P Institute Go Exome Sequencing, G. Jondeau, D.M. Milewicz, TGFB2 mutations cause familial thoracic aortic aneurysms and dissections associated with mild systemic features of Marfan syndrome, Nat. Genet 44 (2012) 916–921. [PubMed: 22772371]

[35]. Judge DP, Biery NJ, Keene DR, Geubtner J, Myers L, Huso DL, Sakai LY, Dietz HC, Evidence for a critical contribution of haploinsufficiency in the complex pathogenesis of Marfan syndrome, J. Clin. Invest 114 (2004) 172–181. [PubMed: 15254584]

[36]. Ishtiaq Ahmed AS, Bose GC, Huang L, Azhar M, Generation of mice carrying a knockout-first and conditional-ready allele of transforming growth factor beta2 gene, Genesis 52 (2014) 817–826. [PubMed: 24895296]

[37]. Markowitz D, Goff S, Bank A, Construction and use of a safe and efficient amphotropic packaging cell line, Virology 167 (1988) 400–406. [PubMed: 2462307]

[38]. Sanford LP, Ormsby I, Gittenberger-de Groot AC, Sariola H, Friedman R, Boivin GP, Cardell EL, Doetschman T, TGFbeta2 knockout mice have multiple developmental defects that are non-overlapping with other TGFbeta knockout phenotypes, Development 124 (1997) 2659–2670. [PubMed: 9217007]

[39]. Liu J, Tseu I, Wang J, Tanswell K, Post M, Transforming growth factor beta2, but not beta1 and beta3, is critical for early rat lung branching, Dev. Dyn 217 (2000) 343–360. [PubMed: 10767079]

[40]. Milewicz DM, Braverman AC, De Backer J, Morris SA, Boileau C, Maumenee IH, Jondeau G, Evangelista A, Pyeritz RE, Marfan syndrome, Nat. Rev. Dis. Primers 7 (2021) 64. [PubMed: 34475413]

[41]. Neubauer J, Haas C, Bartsch C, Medeiros-Domingo A, Berger W, Post-mortem whole-exome sequencing (WES) with a focus on cardiac disease-associated genes in five young sudden unexplained death (SUD) cases, Int. J. Legal Med 130 (2016) 1011–1021. [PubMed: 26846766]

[42]. Doetschman T, Georgieva T, Li H, Reed TD, Grisham C, Friel J, Estabrook MA, Gard C, Sanford LP, Azhar M, Generation of mice with a conditional allele for the transforming growth factor beta3 gene, Genesis 50 (2012) 59–66. [PubMed: 22223248]

[43]. Shull MM, Ormsby I, Kier AB, Pawlowski S, Diebold RJ, Yin M, Allen R, Sidman C, Proetzel G, Calvin D, et al. , Targeted disruption of the mouse transforming growth factor-beta 1 gene results in multifocal inflammatory disease, Nature 359 (1992) 693–699. [PubMed: 1436033]

[44]. Phoon CKL, Turnbull DH, Cardiovascular Imaging in Mice, Curr. Protoc. Mouse Biol 6 (2016) 15–38. [PubMed: 26928662]

[45]. Chen W, Van Beusecum JP, Xiao L, Patrick DM, Ao M, Zhao S, Lopez MG, Billings FTT, Cavinato C, Caulk AW, Humphrey JD, Harrison DG, Role of Axl in target organ inflammation and damage due to hypertensive aortic remodeling, Am. J. Physiol. Heart Circ. Physiol 323 (2022) H917–H933. [PubMed: 36083796]

[46]. Gleason RL, Gray SP, Wilson E, Humphrey JD, A multi-axial computer-controlled organ culture and biomechanical device for mouse carotid arteries, J. Biomech. Eng 126 (2004) 787–795. [PubMed: 15796337]

[47]. Ferruzzi J, Bersi MR, Humphrey JD, Biomechanical phenotyping of central arteries in health and disease: advantages of and methods for murine models, Ann. Biomed. Eng 41 (2013) 1311–1330. [PubMed: 23549898]

[48]. Korneva A, Humphrey JD, Maladaptive aortic remodeling in hypertension associates with dysfunctional smooth muscle contractility, Am. J. Physiol. Heart Circ. Physiol 316 (2019) H265–H278. [PubMed: 30412437]

[49]. Yie TA, Loomis CA, Nowatzky J, Khodadadi-Jamayran A, Lin Z, Cammer M, Barnett C, Mezzano V, Alu M, Novick JA, Munger JS, Kugler MC, Hedgehog and PDGF Signaling Intersect During Postnatal Lung Development, Am. J. Respir. Cell Mol. Biol (2023).

Author Manuscript Author Manuscript Author Manuscript Author Manuscript

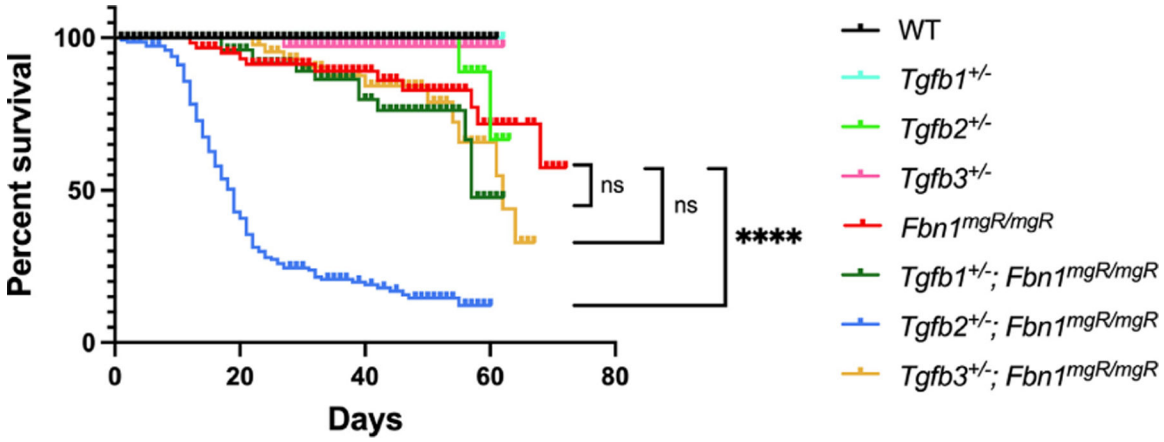

Fig. 1.

Haploinsufficiency of TGF-β2 promotes premature death in *Fbn1*$^{mgR/mgR}$ mice. Kaplan Meier survival curves of WT (*n* = 61), *Tgfb1*$^{+/-}$ (*n* = 62), *Tgfb2*$^{+/-}$ (*n* = 63), *Tgfb3*$^{+/-}$ (*n* = 62), *Fbn1*$^{mgR/mgR}$ (n = 71), *Tgfb1*$^{+/-}$; *Fbn1*$^{mgR/mgR}$ (n = 66), *Tgfb2*$^{+/-}$; *Fbn1*$^{mgR/mgR}$ (*n* = 151), and *Tgfb3*$^{+/-}$; *Fbn1*$^{mgR/mgR}$(*n* = 67) mice. The differences between *Fbn1*$^{mgR/mgR}$ and WT or *Tgfb2*$^{+/-}$; *Fbn1*$^{mgR/mgR}$ mice survival were statistically significant (p <0.0001). There was no statistically significant difference in survival between *Fbn1*$^{mgR/mgR}$ and *Tgfb1*$^{+/-}$; *Fbn1*$^{mgR/mgR}$ mice (p = 0.2324) or *Tgfb3*$^{+/-}$; *Fbn1*$^{mgR/mgR}$ mice (p = 0.2642).

Author Manuscript Author Manuscript Author Manuscript Author Manuscript

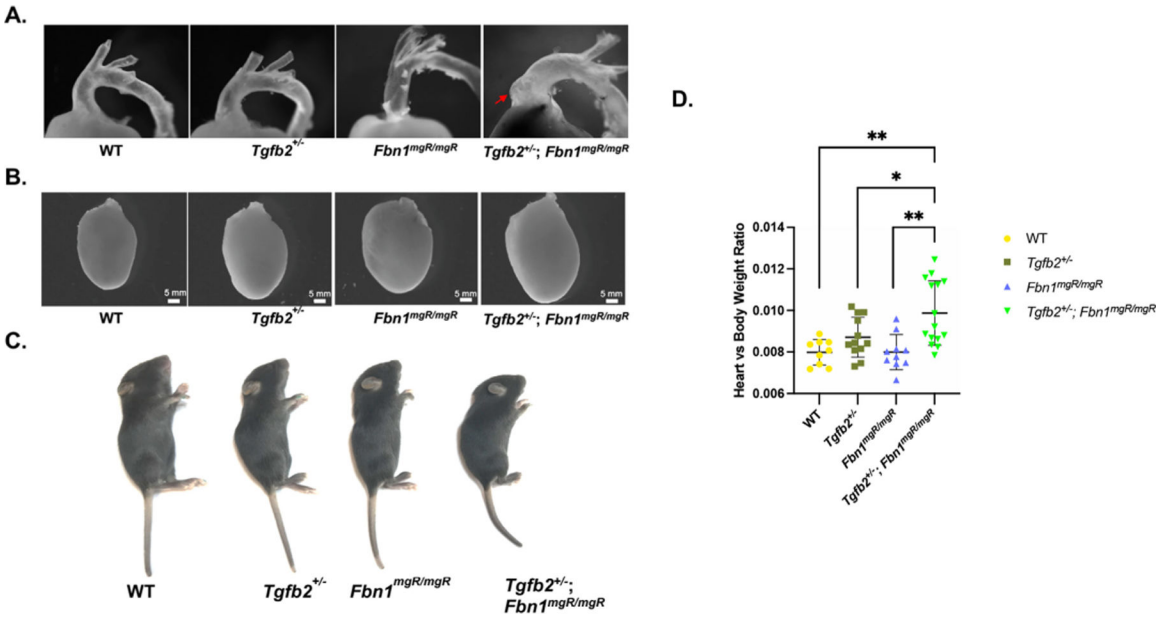

Fig. 2.

Reduction of a single copy of *Tgfb*2 promotes cardiomegaly and aneurysm in *Fbn1*$^{mgR/mgR}$ mice. (A) Gross morphology of the ascending aorta in WT, *Tgfb2*$^{+/-}$, *Fbn1*$^{mgR/mgR}$, and *Tgfb2*$^{+/-}$; *Fbn1*$^{mgR/mgR}$ mice. *Tgfb2*$^{+/-}$; *Fbn1*$^{mgR/mgR}$ mice typically develop ascending aortic aneurysms (single red arrow) by P12, whereas, age-matched *Fbn1*$^{mgR/mgR}$ mice rarely had aneurysms. (B) Macroscopic examination of WT, *Tgfb2*$^{+/-}$, *Fbn1*$^{mgR/mgR}$, or *Tgfb2*$^{+/-}$; *Fbn1*$^{mgR/mgR}$ hearts indicating a larger heart size in *Tgfb2*$^{+/-}$; *Fbn1*$^{mgR/mgR}$ mice. (C) Body size of WT, *Tgfb2*$^{+/-}$, *Fbn1*$^{mgR/mgR}$, and

Author Manuscript Author Manuscript Author Manuscript Author Manuscript

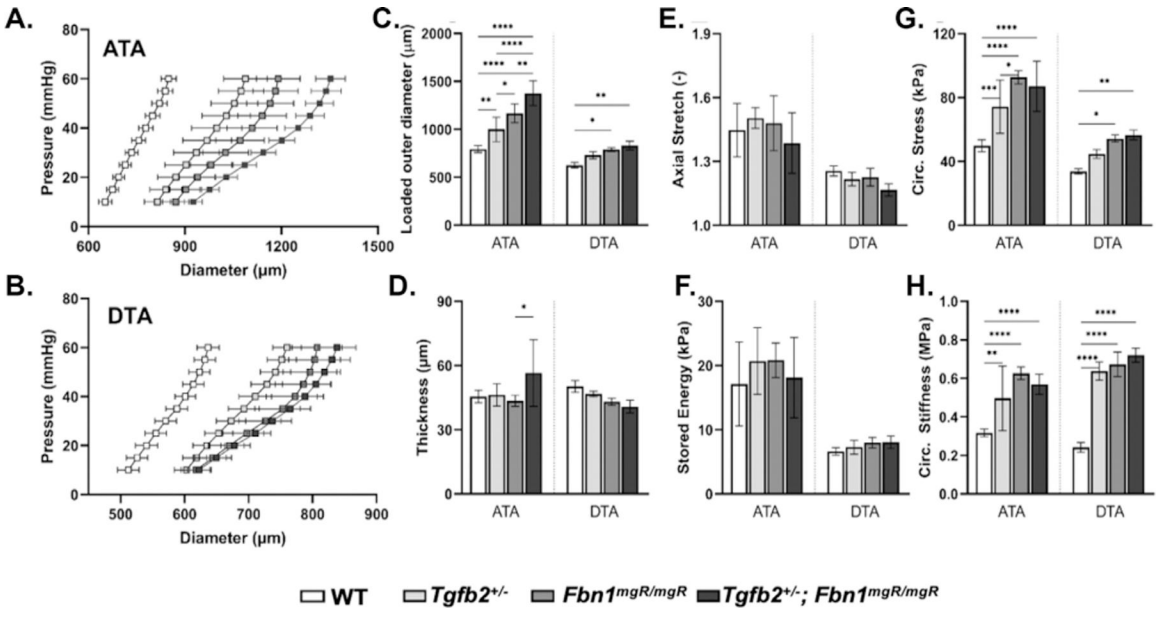

Fig. 3.

(A, B) Structural properties and key (C, D) geometric and (E, H) mechanical metrics for the ascending (ATA) and descending (DTA) thoracic aorta at P12 for the four primary genotypes: WT, *Tgfb2*$^{+/-}$, *Fbn1*$^{mgR/mgR}$, and *Tgfb2*$^{+/-}$; *Fbn1*$^{mgR/mgR}$ mice. Data are shown as mean SEM (n = 5 per group), with statistical significance determined via ANOVA and post-hoc Bonferroni testing.

Author Manuscript Author Manuscript Author Manuscript Author Manuscript

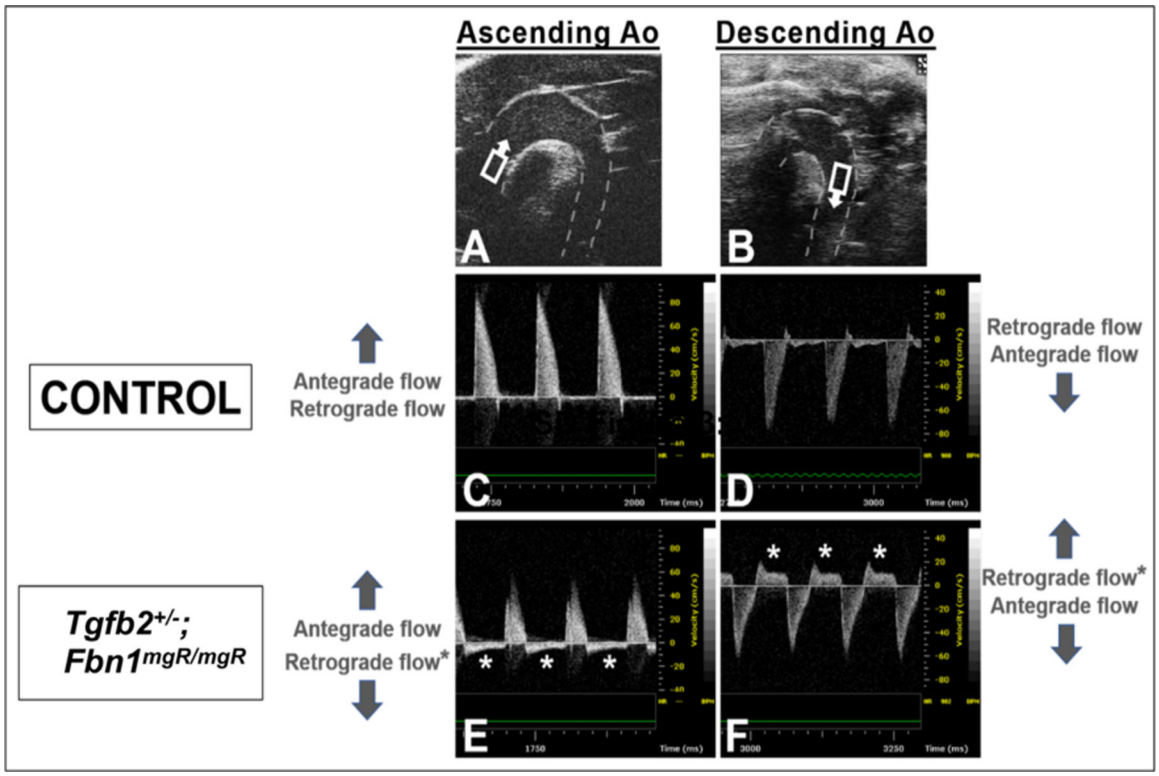

Fig. 4.

Abnormally regurgitant aortic flow in compound *Tgfb2*$^{+/-}$; *Fbn1*$^{mgR/mgR}$ mice observed with echo-Doppler analysis. (A, B) Ultrasound images of the aortic arch, with pulsed-wave spectral Doppler sample volumes placed schematically in the ascending and proximal descending thoracic aorta. In control mice, there is normal Doppler flow in the ascending aorta (C) and descending aorta (D), with all-antegrade flow and no retrograde (reversed) flow. However, in *Tgfb2*$^{+/-}$; *Fbn1*$^{mgR/mgR}$ mutant mice, retrograde flow is evident (asterisks) in both the ascending (E) and descending aorta (F).

Author Manuscript Author Manuscript Author Manuscript Author Manuscript

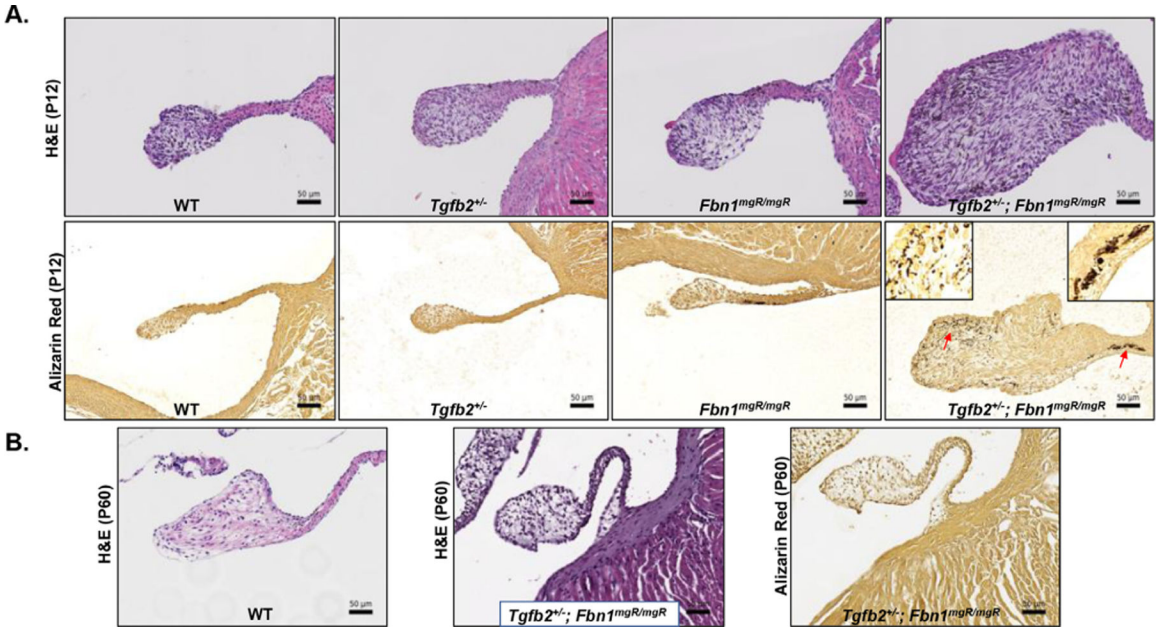

Fig. 5.

Tgfb2 haploinsufficiency promotes aortic leaflet abnormalities in $Tgfb2^{+/-}$; $Fbn1^{mgR/mgR}$ mice. (A) H&E- and Alizarin Red-stained aortic valve leaflets. H&E-stained sections from P12 WT, $Tgfb2^{+/-}$, $Fbn1^{mgR/mgR}$ and $Tgfb2^{+/-}$; $Fbn1^{mgR/mgR}$ littermates indicate that at this time $Tgfb2^{+/-}$; $Fbn1^{mgR/mgR}$ mice have significantly larger aortic leaflets compared to age matched WT, $Tgfb2^{+/-}$, or $Fbn1^{mgR/mgR}$ mice. Dark red/brown nodules identified by Alizarin Red staining are indicative of calcification in both $Fbn1^{mgR/mgR}$ and $Tgfb2^{+/-}$; $Fbn1^{mgR/mgR}$ mice. Inserts show higher magnification (3X) of calcium deposits in $Tgfb2^{+/-}$; $Fbn1^{mgR/mgR}$ mice. Red arrows indicate regions of high calcification (B) $Tgfb2^{+/-}$; $Fbn1^{mgR/mgR}$ mice that survived for 60 days have normal aortic leaflets with no calcification.

Author Manuscript Author Manuscript Author Manuscript Author Manuscript

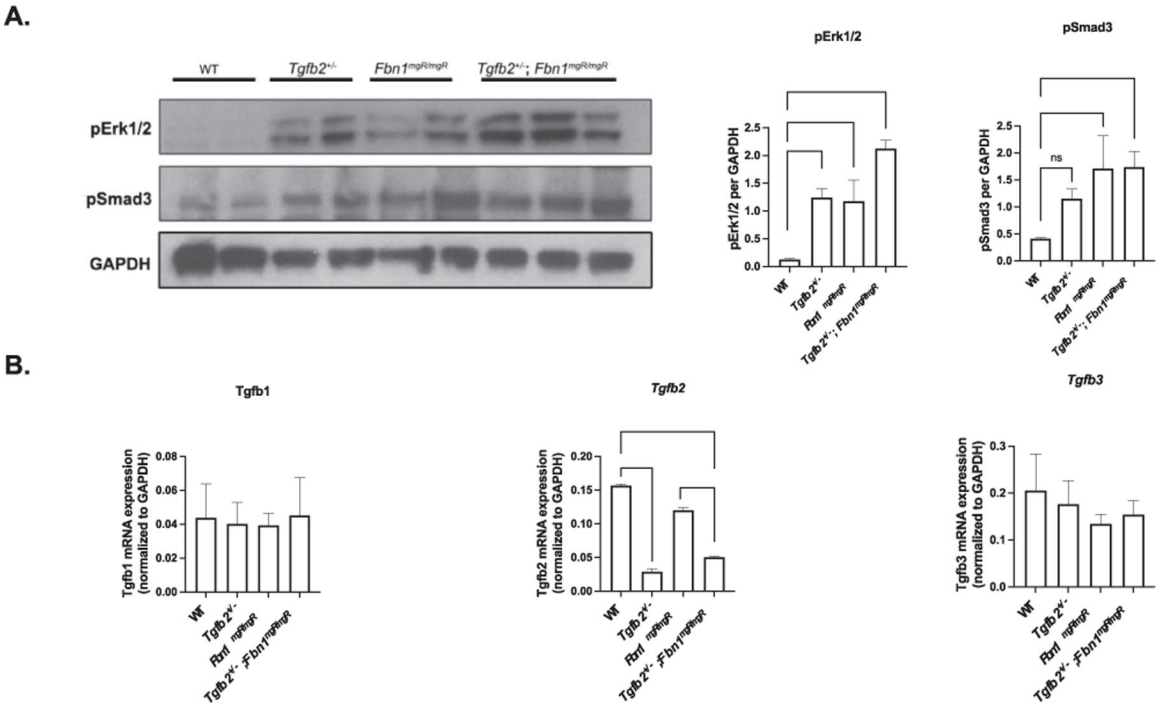

Fig. 6.

Tgfb transcription and signaling in aortic tissue. (A) Aortic extracts from WT, *Tgfb2*$^{+/-}$, *Fbn1*$^{mgR/mgR}$, and *Tgfb2*$^{+/-}$; *Fbn1*$^{mgR/mgR}$ mice were prepared, and probed with antibodies to pErk and pSmad3 by immunoblotting after SDS gel electrophoresis. The quantification of the bands and normalization to the GAPDH control revealed that signaling for both markers was relatively low in WT, but increased in *Tgfb2*$^{+/-}$, *Fbn1*$^{mgR/mgR}$, and *Tgfb2*$^{+/-}$; *Fbn1*$^{mgR/mgR}$ samples. The illustration is representative of one of 3 gels, all of which gave similar results. (B) Q-RT-PCR was performed using RNA extracted from the aortas of WT, *Tgfb2*$^{+/-}$, *Fbn1*$^{mgR/mgR}$, and *Tgfb2*$^{+/-}$; *Fbn1*$^{mgR/mgR}$ mice. mRNA expression (normalized to GAPDH) was determined. The results indicate that *Tgfb1* and *3* were transcribed at similar levels in WT, *Tgfb2*$^{+/-}$, *Fbn1*$^{mgR/mgR}$, and *Tgfb2*$^{+/-}$; *Fbn1*$^{mgR/mgR}$ tissue. *Tgfb2* transcription was significant in WT and *Fbn1*$^{mgR/mgR}$ samples, but was reduced in the *Tgfb2*$^{+/-}$ and *Tgfb2*$^{+/-}$; *Fbn1*$^{mgR/mgR}$ samples. The figure represents averages from the results of 3 experiments, each of which was run with triplicate samples.

Author Manuscript Author Manuscript Author Manuscript Author Manuscript

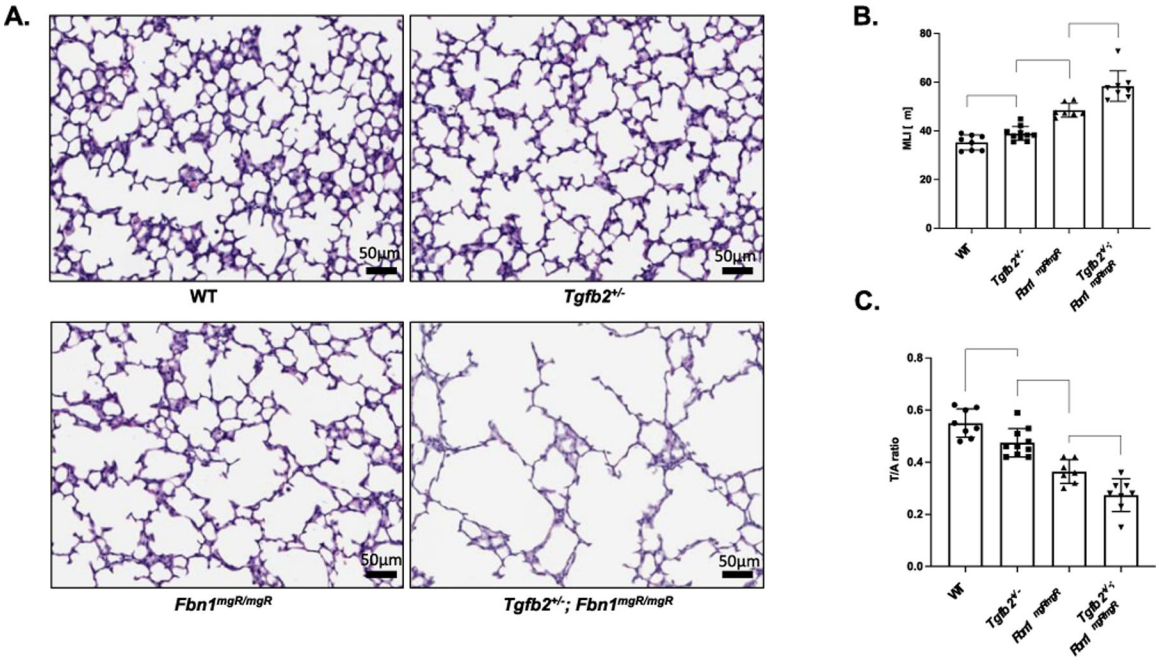

Fig. 7.

Morphology and morphometry of postnatal lungs at P12 from WT, *Tgfb2*$^{+/-}$, *Fbn1*$^{mgR/mgR}$ and *Tgfb2*$^{+/-}$; *Fbn1*$^{mgR/mgR}$ mice. Lungs of WT, *Tgfb2*$^{+/-}$, *Fbn1*$^{mgR/mgR}$, and *Tgfb2*$^{+/-}$; *Fbn1*$^{mgR/mgR}$ littermates were prepared as described in Methods. Scanned lung cross-sections were evaluated by morphologic (Panel A) and morphometric analysis (Panels B and C). As expected, *Fbn1*$^{mgR/mgR}$ lungs have enlarged alveolar airspaces, when compared with WT or *Tgfb2*$^{+/-}$ samples. This phenotype is further exacerbated in *Tgfb2*$^{+/-}$; *Fbn1*$^{mgR/mgR}$ mice that have lungs with a saccular appearance with few alveolar septa when compared with *Fbn1*$^{mgR/mgR}$ lungs. Increased mean linear intercept (MLI) and decreased T/A ratio values are seen in *Tgfb2*$^{+/-}$; *Fbn1*$^{mgR/mgR}$ when compared with *Fbn1*$^{mgR/mgR}$ mice. Data: normalized means +/− SD, Scale bar: 50 μm.

Author Manuscript Author Manuscript Author Manuscript Author Manuscript

Table 1.

Quantitation of survivors for WT, *Tgfb2*$^{+/-}$, *Fbn1*$^{mgR/mgR}$, and *Tgfb2*$^{+/-}$; *Fbn1*$^{mgR/mgR}$ mice before or after postnatal day 20.

	WT	*Tgfb2* $^{+/-}$	*Fbn1* $^{mgR/mgR}$	*Tgfb2*$^{+/-}$; *Fbn1*$^{mgR/mgR}$
Total animals	61	63	71	151
Deaths due to hemothorax	–	–	7/38 < P20 27/38 > P20	6/59 > P20
Deaths due to other factors	–	2/63 > P20	2/38 < P20 2/38 > P20	52/59 < P20 1/59 > P20

Table 1. Hemothorax in necropsied WT, *Tgfb2*$^{+/-}$, *Fbn1*$^{mgR/mgR}$, and *Tgfb2*$^{+/-}$; *Fbn1*$^{mgR/mgR}$ mice. Upper row - total number of animals of each genotype in the study. Middle row - number of animals with hemothorax over the total number of animals necropsied. Bottom row - number of animals that died from a cause other than hemothorax. Not all animals that died were analyzed, as some were eaten and some had decomposed by the time of discovery. Number of animals that died before and after P20 is indicated by the numbers within the brackets.

Matrix Biol. Author manuscript; available in PMC 2023 September 27.

Author Manuscript Author Manuscript Author Manuscript Author Manuscript

Table 2.

Echocardiographic functional analysis for WT, *Tgfb2*$^{+/-}$, *Fbn1*$^{mgR/mgR}$ and *Tgfb2*$^{+/-}$; *Fbn1*$^{mgR/mgR}$ double mutant mice.

	WT n = 6	***Tgfb2*$^{+/-}$ n =6**	***Fbn1*$^{mgR/mgR}$ n= 13**	***Tgfb2*$^{+/-}$; *Fbn1*$^{mgR/mgR}$ "All" n=8**	***Tgfb2*$^{+/-}$; *Fbn1*$^{mgR/mgR}$ "Normal" n =3**	***Tgfb2*$^{+/-}$; *Fbn1*$^{mgR/mgR}$ "Abnormal" n = 5**
Age (Postnatal days)	13.00 ± 0.89	12.67 ± 0.82	12.38 ± 0.65	12.67 ± 0.87	12.67 ± 1.15	12.80 ± 0.84
Body mass (g)	8.24 ± 1.14	7.46 ± 1.46	7.56 ± 1.42	7.73 ± 1.20	7.48 ± 0.42	7.81 ± 1.64
Aortic root (mm)	1.24 ± 0.12	1.30 ± 0.16	1.38 ± 0.15	1.79 ± 0.43	1.51 ± 0.27	2.03 ± 0.41
Ascending aorta (mm)	0.97 ± 0.10	1.02 ± 0.13	1.09 ± 0.15	1.30 ± 0.28	1.04 ± 0.15	1.46 ± 0.20
Left ventricular diastolic dimension (mm)	2.53 ± 0.35	2.70 ± 0.54	2.51 ± 0.33	2.97 ± 0.66	2.37 ± 0.16	3.33 ± 0.56
Fractional shortening	0.49 ± 0.07	0.44 ± 0.10	0.55 ± 0.09	0.44 ± 0.15	0.57 ± 0.02	0.36 ± 0.14
Mice with any abnormal retrograde aortic flow (AAO or DAO)	0/6	1/6	2/13	5/8	0/3	5/5
Mice with moderate or severe retrograde aortic flow (AAO or DAO)	0/6	0/6	0/13	4/8	0/3	4/5

Table 2. Transthoracic echocardiographic measurements. Transthoracic echocardiographic examination of WT, *Tgfb2*$^{+/-}$, *Fbn1*$^{mgR/mgR}$, and *Tgfb2*$^{+/-}$; *Fbn1*$^{mgR/mgR}$ mice (P12-P14) was performed to determine the diameters of the aortic root (mm) and ascending aorta (mm), LV diastolic dimension (mm), fractional shortening, and retrograde aortic flow. *Tgfb2*$^{+/-}$; *Fbn1*$^{mgR/mgR}$ mice have aortic regurgitation as well as statistically larger left ventricles (LV) and aortic aneurysm dimensions. LV dimensions were significantly increased in *Tgfb2*$^{+/-}$; *Fbn1*$^{mgR/mgR}$ mice with aortic regurgitation vs without aortic regurgitation (p<0.01).

Matrix Biol. Author manuscript; available in PMC 2023 September 27.